Arabian Journal of Chemistry (2022) 15, 103919

King Saud University

Arabian Journal of Chemistry

www.ksu.edu.sa
www.sciencedirect.com

ORIGINAL ARTICLE

The novel 4-hydroxyphenylpyruvate dioxygenase inhibitors in vivo and in silico approach: 3D-QSAR analysis, molecular docking, bioassay and molecular dynamics

Juan Shi [1], Li-Xia Zhao [1], Jia-Yu Wang, Tong Ye, Meng Wang, Shuang Gao, Fei Ye [*], Ying Fu [*]

Department of Chemistry, College of Arts and Sciences, Northeast Agricultural University, Harbin 150030, China

Received 16 March 2022; accepted 10 April 2022
Available online 18 April 2022

KEYWORDS

HPPD inhibitors;
3D-QSAR;
Molecular docking;
Molecular dynamics;
Bioassay

Abstract 4-Hydroxyphenylpyruvate dioxygenase (HPPD) is not only an important target enzyme for the treatment of type I tyrosinemia, but also a new target for design bleaching herbicides, and it plays key role in the biosynthesis of tocopherol and plastoquinone. Thirty-six known active pyridine derivatives were collected, and comparative molecular field analysis (CoMFA) and comparative molecular similarity index analysis (CoMSIA) models based on common skeleton were constructed to obtain novel HPPD herbicides with higher activity. Two new HPPD inhibitors were rationally designed and synthesized according to the CoMFA and CoMSIA models and verified by enzyme activity, biological assays, and molecular docking. The promising compound **W1** ((*E*)-5-(3-(4-bromophenyl)acryloyl)-6-hydroxy-2,3-dihydropyridin-4(1H)-one) showed better *At*HPPD inhibitory activity, and the bioassay results revealed that some weeds showed bleaching symptoms. The good binding stability of **W1** and protein was confirmed by molecular dynamics simulation in 100 ns. These results would be highly useful in the progress of new HPPD inhibitors discovery.

[*] Corresponding authors at: Department of Chemistry, College of Arts and Sciences, Northeast Agricultural University, Harbin 150030, China.
E-mail addresses: Shijuan1233@163.com (J. Shi), zhaolixia@neau.edu.cn (L.-X. Zhao), wangjiayu9819@163.com (J.-Y. Wang), yetong0812@163.com (T. Ye), wangmengwm0922@163.com (M. Wang), gaoshuang@neau.edu.cn (S. Gao), yefei@neau.edu.cn (F. Ye), fuying@neau.edu.cn, yefei@neau.edu.cn, fuying@neau.edu.cn (Y. Fu).
[1] These authors contributed equally to this work.

Peer review under responsibility of King Saud University.

ELSEVIER Production and hosting by Elsevier

https://doi.org/10.1016/j.arabjc.2022.103919
1878-5352

1. Introduction

4-Hydroxyphenylpyruvate dioxygenase (HPPD) is an important enzyme in the course of tyrosine metabolism in organisms, and it exists in almost all aerobic organisms (Liang et al., 2020). HPPD is not only an important target remedy for the treatment of type I tyrosinemia, but also an effective target for design herbicides (Hu et al., 2022). HPPD is an oxygenase with iron-dependent nonheme in the 2-His-1-carboxylate facial triad family (Lin et al., 2019a; Raspail et al., 2011; He et al., 2019). HPPD catalyzes the complex conversion of 4-hydroxyphenylpyruvate (HPPA) to homogenate acid (HGA) and plays an important role in the biosynthesis of cofactors plasmoquinone and tocopherol in plants (Li et al., 2021; Wang et al., 2021; Moran, 2014). Photosynthetic damage is due to the inhibition of HPPD-catalyzed reactions in chloroplasts, which leads to leaf bleaching followed by weed necrosis and death (Neidig et al., 2004; Fu et al., 2019a). HPPD inhibitors mainly include pyrazoles, triketones, isoxazoles and others (Ndikuryayo et al., 2017). In particular, the novel pyrazoline-quinazoline-2, 4-diketone hybrids showed good herbicidal activity (He et al., 2020). The newly developed 3-hydroxy-2-(3,5,6-trichloro-4–((4-isopropylbenzyl)amino)picolinoyl) cyclohexyl-2-en-1-one is 5.8-fold more active than the commercially available mesotrione (Nan et al., 2021). The advantages of HPPD inhibitors are their excellent bioactivity, low residue accumulation, broad-spectrum weed control, environmental friendliness, low toxicity, and safe application (Aouidate et al., 2018; Shaner et al., 2004; Wang et al., 2020a; Jia et al., 2019). Hence, the study of novel HPPD inhibitors has been recognized as one of the most promising targets in the field of herbicides (Qu et al., 2021; Lin et al., 2021).

Based on the known crystal structure of HPPD and molecular information of HPPD inhibitors, potential inhibitors can be better validated by molecular docking and molecular dynamics (Sabine et al., 2020; Fu et al., 2020; Singh et al., 2018), which exhibits key features in ligand-receptor binding interactions and enables virtual screening of many compound databases (Xing et al., 2020; Ganesan et al., 2018). These workflows are efficient to identify suitable and potent inhibitors by considering the mechanism of activity prior to the experiment (Sushil et al., 2021). In the past few decades, quantitative structure activity relationship (QSAR) models are an effective calculation tool in drug design and have been widely applied to predict the bioactive compounds (Zhang et al., 2010; Tang et al., 2016; Wang et al., 2017; Dong et al., 2017; Fu et al., 2019b; Mohd et al., 2019). Comparative molecular field analysis (CoMFA) and comparative molecular similarity index analysis (CoMSIA) models were established based on a series of sulfa derivatives, and 35 potential inhibitors against tomato chlorosis virus were successfully developed (Jiang et al., 2021). Cloud 3D-QSAR provides a one-stop solution for molecular interaction field (MIF) calculation and result analysis of integrated molecular structure generation, alignment, and molecular interactions (Wang et al., 2020c).

QSAR combined with molecular docking and molecular dynamics (MD) simulation is a valid means of obtaining highly accurate information about the interactions between ligands and receptors (Liu et al., 2019; Singh et al., 2016; Kothandan et al., 2011). Molecular dynamics helps optimize the understanding of protein function to accelerate drug discovery (Yang et al., 2019). It also provides powerful insights to develop novel herbicides for target enzymes (Huang et al., 2018; Wang et al., 2020b).

In the current study, a group of potential HPPD inhibitors with common skeletons were selected to establish CoMFA and CoMSIA models. Contour maps were employed to guide the design and synthesis of two potential compounds with improved predictive activity. The two synthesized compounds were tested in vivo, and bioassays were performed to verify their bioactivity. Molecular docking and MD studies were employed to analyze and confirm the stability of the receptor–ligand complex and to provide more messages at the binding site.

2. Materials and methods

2.1. Information collection and generation of 3D-QSAR models

In the present study, 36 reported pyridine derivatives were collected as *At*HPPD inhibitors (Table 1) (Fu et al., 2019c; Fu et al., 2021). Out of 36 compounds, 29 were randomly chosen as the training set to build the model, and the surplus 6 compounds served as the test set to assess the model. These compounds were selected to cover the entire range of biological activities.

All 36 compounds were generated the 3D conformations with SYBYL-X 2.0 software. Energy minimization was achieved by a Tripos force field and by applying Gasteiger-Hückel charges. The dataset was imported into the molecular spreadsheet. The maximum number of iterations was 1000, and the Powell gradient energy convergence value was set to 0.005 kcal/mol Å. To obtain good 3D-QSAR model, multiple search method was used to acquire the molecular conformation. Each compound performed 1000 maximum cycles and produced 200 maximum conformations. For the sake of getting an orderly alignment, the lowest energy conformation of the most active compound 1 (2-(6-chloronicotinoyl)-3-hydroxy cyclohex-2-en-1-one) was selected as the superposition template. Remainder molecules of the training set were aligned with the common skeleton. The alignment results were shown in Fig. 1.

The CoMFA and CoMSIA models were constructed with 29 compounds as the training set. pIC_{50} values were selected as the dependent variable for model research. Partial least squares (PLS) regression analysis was applied to generate valid and definite CoMFA and CoMSIA models. The dimensions of the CoMFA fields were calculated by a sp^3 carbon with a + 1.0 charge in the process of steric and electrostatic fielding. The regression analysis was performed using the leave-one-out (*LOO*) cross-validation method. The optimum number of components (*ONC*), cross-validation coefficient (q^2), coefficient of determination (r^2), standard error of estimate (*SEE*) and *F* value were calculated to evaluate the model. Low *SEE* values and high q^2, r^2 and *F* values were necessary for a favorable model.

2.2. Docking study and physicochemical properties

The preparation of the ligands is the same as that of the dataset in the data collection. The X-ray crystal structure of *At*HPPD for molecular docking was gained from the Protein

Table 1 The structures of pyridine derivatives and corresponding experimental and predicted activities.

Compound	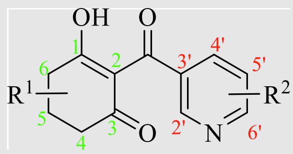		Experimental value		Predicted value (pIC_{50})	
	R^1	R^2	IC_{50} (μM)	pIC_{50}^{a}	CoMFA	CoMSIA
1	H	6′-Cl	0.262	6.582	6.573	6.567
2	5-CH_3	6′-Cl	3.083	5.511	5.607	5.655
*3	5,5-diCH_3	6′-Cl	3.280	5.484	5.475	5.465
4	5-Ph	6′-Cl	4.498	5.347	5.362	5.258
5	H	2′-CF_3	2.215	5.655	5.676	5.698
6	5-CH_3	2′-CF_3	3.451	5.462	5.421	5.392
7	5,5-diCH_3	2′-CF_3	4.368	5.360	5.362	5.258
*8	5-Ph	2′-CF_3	10.473	4.980	4.926	4.894
9	H	5′-Br	2.691	5.570	5.59	5.516
10	5-CH_3	5′-Br	4.404	5.356	5.485	5.55
11	5,5-diCH_3	5′-Br	13.985	4.854	4.817	4.814
12	H	6′-F	3.489	5.457	5.437	5.456
13	5-CH_3	6′-F	8.755	5.058	5.074	5.097
14	5-Ph	6′-F	1.905	5.720	5.698	5.787
*15	H	6′-CF_3	0.704	6.152	6.128	6.141
16	5-CH_3	6′-CF_3	0.791	6.102	6.059	6.044
17	5,5-diCH_3	6′-CF_3	4.009	5.397	5.33	5.434
18	5-Ph	6′-CF_3	0.961	6.017	5.912	6.025
19	H	6′-Br	1.731	5.762	5.716	5.759
20	5-CH_3	6′-Br	2.729	5.564	5.593	5.579
21	5,5-diCH_3	6′-Br	11.315	4.946	4.926	4.894
*22	5-Ph	6′-Br	0.920	6.036	6.047	6.026
23	H	5′-Cl, 6′-Cl	1.024	5.990	5.953	5.893
24	5-CH_3	5′-Cl, 6′-Cl	1.616	5.792	5.78	5.698
25	5,5-diCH_3	5′-Cl, 6′-Cl	1.940	5.712	5.698	5.787
	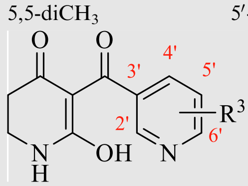		Experimental value		Predicted value (pIC_{50})	
	R^3		IC_{50} (μM)	pIC_{50}	CoMFA	CoMSIA
26	6′-Br		1.157	5.937	6.014	5.944
27	5′-Cl, 6′-Cl		0.959	6.018	5.912	6.025
28	5′- Br, 6′-Cl		0.470	6.328	6.244	6.282
*29	5′-F		1.720	5.764	5.707	5.782
30	5′-Cl		1.590	5.799	5.834	5.775
31	5′-Br		1.347	5.871	5.836	5.982
32	2′-CF_3		2.238	5.650	5.698	5.731
*33	6′-CF_3		1.423	5.847	5.721	5.634
34	H		8.556	5.068	5.088	5.104
35	6′-F		1.318	5.880	5.853	5.863
36	6′-Cl		1.267	5.897	5.952	5.909

Note: [a] pIC_{50} = -lg (IC_{50}), calculated with the average value of IC_{50}, IC_{50}: Half maximal inhibitory concentration toward *At*HPPD.
*Compounds were considered as the test set.

Data Bank (PDB ID: 5YWG) (Lin et al., 2019b). Protein preparation was accomplished by applying the "Prepare Protein" module in Discovery Studio (DS) (Biovia Inc. San Diego, CA, USA, 2020). All water and heteroatoms were deleted from the crystal structure, supplementing missing atoms in residues. The CHARMM force field was used to protonate the structure of HPPD and optimized the conformation of the side chain residues with missing atoms. The binding sites were determined by the cavity position of the co-crystallized ligand in the incipient crystal structure of HPPD.

The co-crystalline ligand mesotrione was redocked to determine whether the CDOCKER program matched the system. The physicochemical properties of the compounds were calculated by the "Calculate Molecular Properties" module of DS.

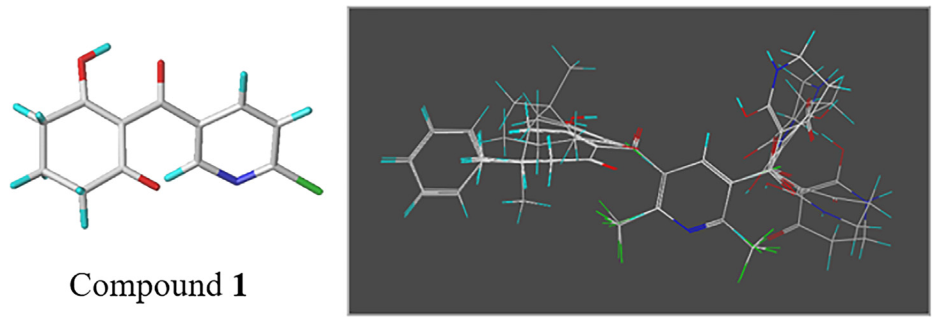

Fig. 1 3D-QSAR molecular superposition of the training and test sets using compound 1 as the template.

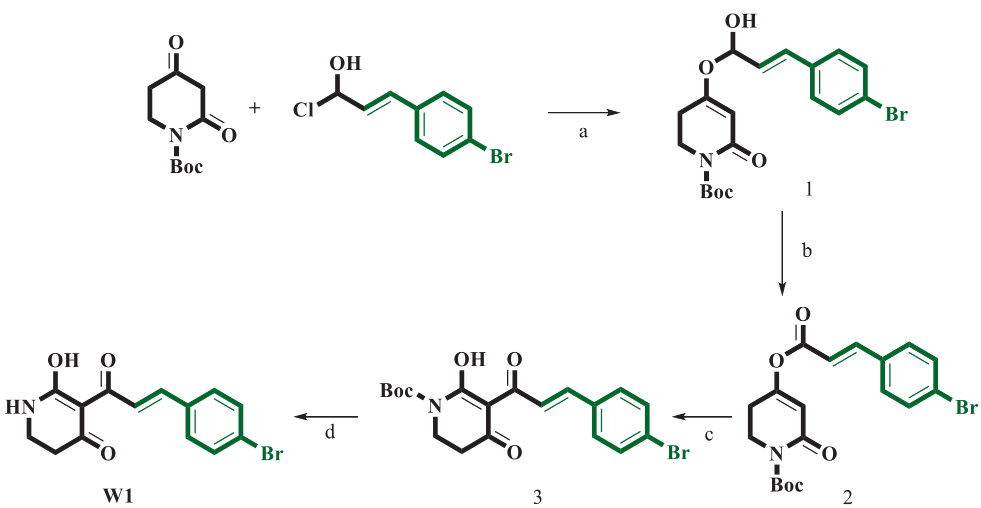

(a) $SOCl_2$, reflux, 2.5h, reflux
(b) tert-butyl 2,4-dioxopiperidine-1-carboxylate, Et_3N, $SmCl_3$, 1h, 0℃
(c) acetone cyanohydrin, Et_3N, acetonitrile, 12h, rt
(d) TFA, 1h, 0℃

Scheme 1 Route for the synthesis of compound **W1.**

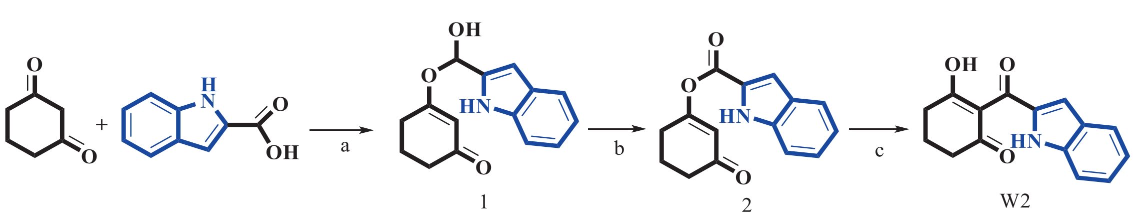

(a) oxalyl chloride, 1h, rt
(b) 1,3-cyanohydrin, pyridine, 0.5h, 0℃
(c) acetone cyanohydrin, Et3N, acetonitrile, 5h, rt

Scheme 2 Route for the synthesis of compound **W2.**

2.3. Chemical synthesis

The synthetic routes to the compounds (**W1** and **W2**) are depicted in Schemes 1 and 2. The detailed synthetic methods are provided in the Supporting Information.

2.4. HPPD inhibitory in vitro assays and herbicidal assays

The HPPD inhibitory activity in vitro was tested by the coupling method. Measurements were executed in 96-well plates (30 ℃) using a microplate reader, and the UV absorption peak was set to 318 nm. Each group of experiments was performed in three replicates and was averaged. The total reaction mixture volume of 200 μL contained 1 mM (20 μL) HPPA, 20 mM (20 μL) sodium ascorbate, 1 mM (20 μL) $FeCl_2$, 20 mM HEPES buffer (NaOH adjusted pH = 7.0, 4-Hydroxyethylpiperazine ethanesulfonic acid), HGD (40 μL), and HPPD (40 μL). The quantity of HGD added was larger than the amount of HPPD during the experiment to ensure that the reaction was completed. Before performing the measurement, all reactants were hatched at 30 °C for no > 15 min. IC_{50} was obtained from the activity curve of the substrate-inhibitor concentration (Song et al., 2021).

The following broad-leaved weeds were selected to assay the in vivo activity: *Abutilon theophrasti (Abutilon theophrasti Medik, AJ), Amaranthus retroflexus (Amaranthus retroflexus L., AR), Eclipta prostrata (Eclipta prostrata L., EP),* and gramineous weeds: *Setaria viridis (Setaria viridis (L.) Beauv., SF), Digitaria sanguinalis (DigitariaviolascensLink, DS), and Echinochloa crus-galli (Echinochloa crusgalli (L.) Beauv., EC)*. The seeds (85% or higher) germination rate was evenly spread in the potting soil and grown in natural conditions. When the dicotyledonous weeds grew to the 3–4 leaf stage and the monocotyledonous weeds grew to the 1–2 leaf stage, **W1** was dissolved in *N,N*-dimethylformamide containing 1% Tween-80 emulsifier, the concentrate was diluted with deionized water, and plants were sprayed on their stems and leaves after budding in the concentration of 150 g ai/ha. On the third day after treatment, visual evaluations of the plant stems or roots and other factors were performed. 20 Seed of *rice (Oryza sativa L.)* and *wheat (Triticum aestivum L.)* were chosen for crop safety test. The commercial herbicides mesotrione was regarded as positive contrast. When the crop entered the four-leaf stage, the safety test of leaf spray crops was carried out at a concentration of 150 g ai/ha. The visual impairment and growth status of individual plants were regularly observed. After 20 days, the crop safety was evaluated (Wang et al., 2014).

2.5. MD simulations

The Amber 16 package was used for MD simulations, and the Amber ff14SB force field was applied to generate the force field of the protein and ligand. Cobalt ions were processed in a metal center parameter generator, and a side chain model containing cobalt ion with His226, His308 and Glu394 composite was created. The obtained structure was immersed in a TIP3P water cube with a distance of at least 10 Å around the box, and an appropriate amount of counter ions was added to the system to neutralize its charge. The energy minimization, heating and balance of each system were realized by the "Sander" program. In each energy minimum step, the steepest descent algorithm was used for the first 2500 steps, and the conjugate gradient algorithm was used for the last 2500 steps. Then the system was gradually heated to 298 K before reaching 1 ns equilibrium in an isobaric-isothermal (NPT) integrated simulation. In the end, the system was subjected to 100 ns of PMEMD program processing in the NPT at a 2 fs time step. Reference values of root mean square deviation (RMSD) was employed to evaluate the stability of the simulation system.

Molecular mechanics and the Poisson-Boltzmann solvation area (MM-PBSA) were applied to analyze the complex affinity. Prime MM-PBSA calculations were executed using the initial and MD-optimized receptor − ligand complexes. The more negative the value of the binding free energy ΔG_{bind}, the stronger the binding force, which was calculated by applying the MM-PBSA method. Prime MM-PBSA ΔG_{bind}, the binding free energy, was calculated with the formula:

$$\Delta G_{bind} = G_{complex} - G_{receptor} - G_{ligand} \quad (1)$$

2.6. ADMET

ADMET prediction for small molecules was performed in DS software. The following parameters were predicted: Solubility Level, PPB# Prediction, Hepatotoxicity, Aerobic Biodegradability, Mutagenicity, Carcinogenicity, Skin irritancy, and DTP Prediction.

3. Results and discussion

3.1. 3D-QSAR models

The experimental and predicted pIC_{50} values of the CoMFA and CoMSIA models for the training and test sets are shown in Table 1, and their calculated statistical parameters were listed in Table 2. The *ONC* in the CoMFA model was 7, and the q^2 was 0.707 (> 0.5), which certified that the CoMFA model had good predictive ability. In the CoMFA model, *SEE* was 0.128 (less than0.95), and *F* was 224.565, and r^2 was 0.954 (> 0.9), suggesting that the model is capable of fine fitting. The contribution of the steric field was 47.3%, slightly lower than the contribution of the electrostatic field of 52.7%. The CoMSIA model displayed good parameters of r^2 (0.944), *F* test value (172.455), and q^2 (0.657) and low *SEE* (0.184), and

Table 2 Results of the CoMFA and CoMSIA models.

Parameter	CoMFA	CoMSIA	Threshold
q^2	0.707	0.657	> 0.5
ONC	7	7	–
r^2	0.954	0.944	> 0.6
SEE	0.128	0.184	Low value
F	224.565	172.455	High value
r^2_{pred}	0.865	0.853	> 0.6
Steric	47.3	12.7	–
Electrostatic	52.7	26.4	–
Hydrophobic	–	23.1	–
H-bond Donor	–	19.2	–
H-bond Acceptor	–	18.6	–

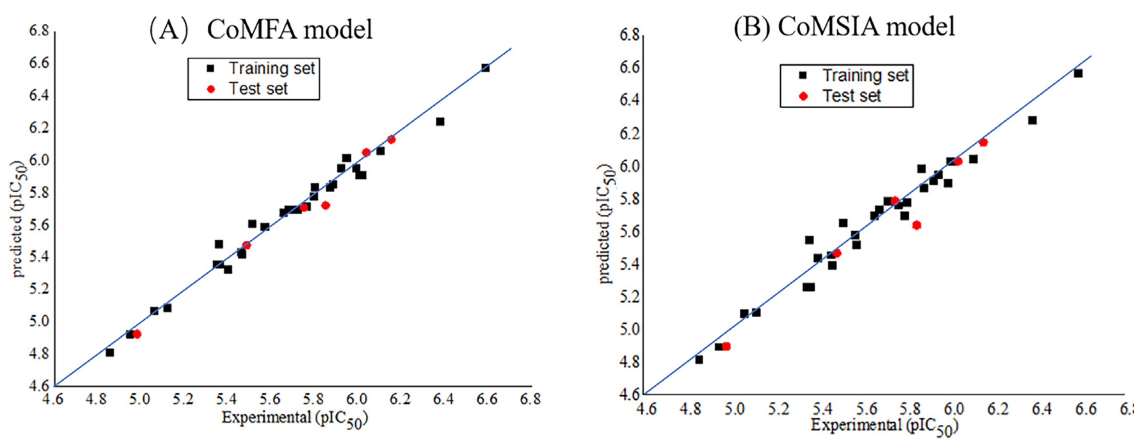

Fig. 2 Experimental and predictive activities of molecules in training and test sets. **(A)** CoMFA model and **(B)** CoMSIA model.

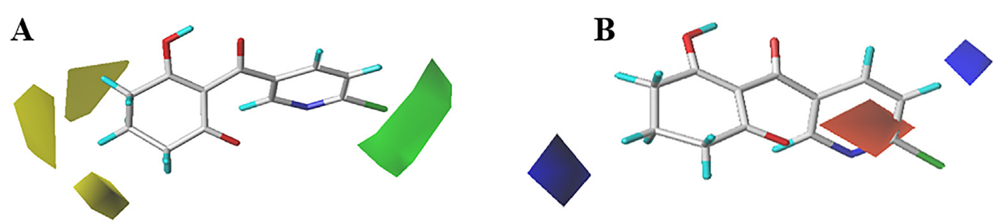

Fig. 3 CoMFA StDev*Coeff contour maps. **(A)** Steric and **(B)** Electrostatic.

the *ONC* was 7. The contributions of steric, electrostatic, hydrophobic, H-bond donor and H-bond acceptor fields were 12.7%, 26.4%, 23.1%, 19.2% and 18.6%, respectively.

Electrostatic field made the greatest contribution in CoMFA model. The electrostatic and hydrophobic fields were found to play major roles in CoMSIA model. In Fig. 2, the black squares and red dots were scattered on both sides of the line $Y = X$, further confirmed that the experimental values of the entire dataset were very close to the predicted values, suggesting the model has superior predictive ability.

3.2. Contour maps analysis of CoMFA models

Compound 1 with the best activity was placed in the contour plot as a reference to explain the effects of various fields on activity. The steric field is shown in Fig. 3**A**, and the green proved that the bulky group was beneficial to the bioactivity of the HPPD inhibitors. In contrast, the small substituents marked in yellow were beneficial for bioactivity. Compounds 1 to 25 were cyclohexanedione derivatives. A small yellow area close to the 5-position of the cyclohexanedione recommended that a small size group at this position had a beneficial effect on inhibition. Compounds exhibited activity when there was no substituent on cyclohexanedione (compounds 1, 5, 9, 12, 15, 19, 23), especially compound 1, which displayed the good activity (Beaudegnies et al., 2009). With the introduction of the methyl group at R^1, the inhibitory activity of the compound was obviously decreased. For example, comparing compounds 1 and 3, the inhibitory activity was obviously reduced because the hydrogen atom at the 5-position of compound 1 (IC_{50} = 0.262 μM) was displayed by a methyl (compound 3, IC_{50} = 3.083 μM). Fig. 3**B** depicts the contour map of the electrostatic descriptor. The electropositive group was favorable for improving the bioactivity of the compounds, as proven by the blue area; in contrast, the electronegative group was favorable for enhancing the bioactivity of the compounds, as indicated by the red area. The red area at the 6-position of the pyridine ring indicated that the electronegative substituents would contribute to the bioactivity of the compounds. Comparing compound 34 with compounds 33, 35 and 36, it was found that the activity was increased when the hydrogen atom at the 6-position of the pyridine ring was substituted by trifluoromethyl, fluorine, or chlorine atoms. These maps were informative in designing new potent and selective HPPD inhibitors.

3.3. Contour maps analysis of CoMSIA models

Steric and electrostatic contour maps of the CoMSIA model were shown in Fig. 4**A and B**, which were greatly analogous to those of the CoMFA model. In Fig. 4**C**, yellow regions with hydrophobic groups were favorable for activity, while white regions corresponding to hydrophilic substitutes were preferred. The R^1-location observation to white, it was advantageous with hydrophilic substitution. A yellow region covered R^2 at the 2-position of the pyridine ring, representing the favorability of hydrophobic features at this position. The introduction of hydrophobic groups provided more potent HPPD inhibitors. For example, the IC_{50} of compounds 1 (6-Cl) and 9(5-Br) were 0.262 μM and 2.69 μM. In the H-bond donor contour map (Fig. 4**D**), the cyan outline indicated a location where the H-bond donor group favored better activity. In contrast, the position of the gray area indicated that H-bond donor experience for lower activity. A small cyan outline was observed near 3-position on cyclohexanedione ring. This suggested that the introducing H-bond donor here was beneficial for increasing activity. The H-bond receptor contour map was shown in Fig. 4**E**, purple and magenta indicated areas where the replacement of H-bond receptor was positive and negative for inhibition. The magenta polyhedron at R^2 on the pyridine ring indicated that the introduction of a H-bond acceptor was unfavorable for the activity. This was consistent with the observation between compounds 12 (6-F, IC_{50} = 3.489 μM) and 19 (6-Br, IC_{50} = 0.731 μM). The H-bond donor and acceptor formed a positive H-bond interaction with the protein, greatly affecting the inhibition of the compound. The IC_{50} of the piperidinedione derivatives (compounds 5, 9, 12, 19 and 23) were lower than those of cyclohexanedione derivatives (compounds 32, 31, 35, 26 and 27), indicating that compounds with piperidinedione subunits possessed better activity than those with cyclohexanedione subunits.

3.4. Design compounds based on CoMFA and CoMSIA models

The structural features favorable for improving the activity are summarized in Fig. 5 on the basis of the information gained by the contour maps. Compounds with piperidinedione as the subunit were more active than those with the cyclohexanedione fragment. It was favorable for the activity by introduction of small sizes, hydrophilic and electropositive substitutions at the 3-, 4- and 5-positions of piperidinedione or cyclohexanedione, and H-bond donors at this district would magnify the activity. The activity was also enhanced with the import of bulky, electronegative and hydrophobic substituents at the 2′-, 5′- and 6′-positions of the pyridine ring. Furthermore, the effect of substituents at the 5′ or 6′ position was better than that at the 2′-position.

In short, bulky and electronegative substitutes of the pyridine ring were favorable, and derivatives of piperidinedione and cyclohexanedione were synthesized. Therefore, four compounds (**W1**, **W2**) were designed in terms of the CoMFA and CoMSIA models. The physicochemical properties of the compounds markedly influenced the biological activity and its interaction with the herbicide target enzyme. Generally, the numbers of H-bond acceptors (HBAs), H-bond donors

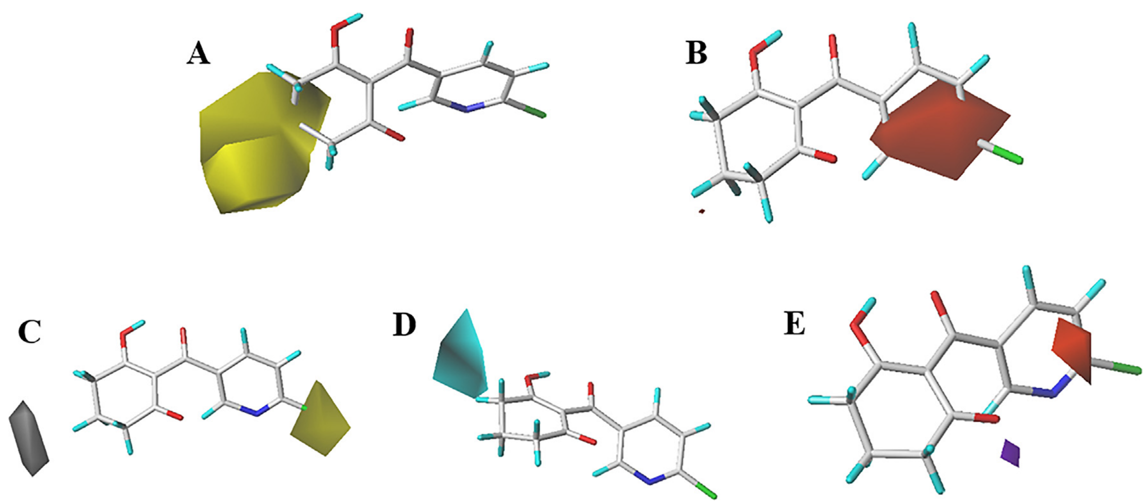

Fig. 4 CoMSIA StDev*Coeff contour maps. **(A)** Steric, **(B)** Electrostatic, **(C)** Hydrophobic, **(D)** H-bond donor and **(E)** H-bond acceptor.

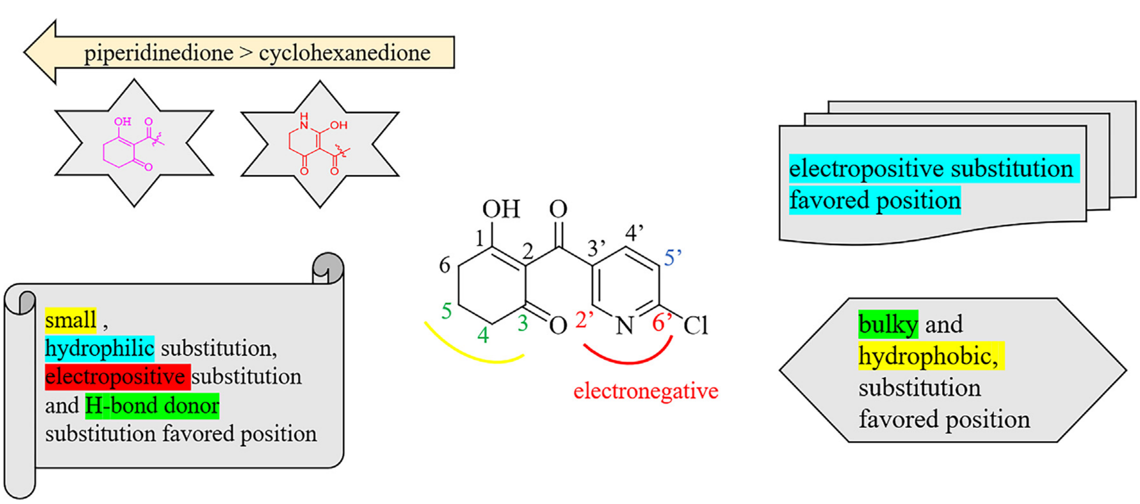

Fig. 5 Summary of the structure–activity relationship.

Table 3 Physicochemical properties of **W1, W2** and mesotrione.

Name	W1	W2	Mesotrione
Structure [a]	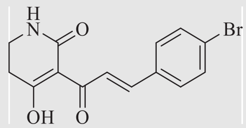	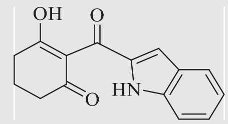	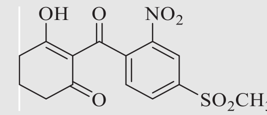
-CDOCKER_ ENERGY [b]	49.02	48.62	42.64
-Interactive energy	58.33	13.14	42.78
Log p [b]	2.46	2.28	1.40
pK_a [b]	3.58	3.13	5.12
MW [a]	322.15	255.27	339.32
HBAs [b]	3	3	4
HBDs [b]	2	1	2
RBs [b]	3	2	4
ARs [b]	1	2	1
SA [b]	322.15	244.92	339.32
Electronegativity [c]	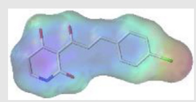	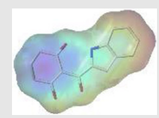	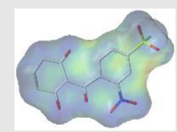

Notes: [a] CS Chemdraw drawing for predicting molecular weight (MW); [b] DS for predicting Log$p$, -CDOCKER_ ENERGY (kcal mol^{-1}), pK_a, rotatable bonds (RB_S), aromatic rings (AR_S), surface area, hydrogen bond acceptors (HBAs) and donors (HBDs); [c] Sybyl-X 6.9 for predicting electronegativity.

Table 4 Inhibitory activity of the compounds against HPPD of different organisms.

Compound	*At*HPPD IC$_{50}$ (μM)	pIC$_{50}$	*h*HPPD IC$_{50}$ (μM)	pIC$_{50}$	*Rice* HPPD IC$_{50}$ (μM)	pIC$_{50}$	*Wheat* HPPD IC$_{50}$ (μM)	pIC$_{50}$
W1	0.201 ± 0.001	6.697	18.394 ± 0.139	4.735	14.877 ± 0.062	4.827	15.631 ± 0.020	4.806
W2	5.221 ± 0.075	5.282	5.067 ± 0.145	5.295	> 100	–	6.582 ± 0.146	5.182
Mesotrione	0.231 ± 0.002	6.636	12.165 ± 0.082	4.915	13.460 ± 0.009	4.871	10.000 ± 0.306	5.000

(HBDs) and aromatic rings (ARs) were positively correlated with the biological activity. Placing emphasis on comparing the physicochemical property of the compounds **W1**, **W2** and mesotrione, it is worth noting that the HBAs, surface area (SA), number of ARs and rotatable bonds (RB), and electronegativity of compounds **W1** and **W2** were quite similar to those of mesotrione (Table 3).

Compared with mesotrione, these compounds also showed a good docking score (-CDOCKER_ENERGY). In order to further demonstrate the reliability of molecular docking, the interactive energy of **W1** was significantly higher than commercial herbicides, indicating the reliability of the model. The predicted pK_a of the obtained compound **W1** was less than 6.0 and even lower than that of mesotrione. Weak acid and low Log p were conducive to the spread of plants and absorption.

All of these results indicated that compound **W1** might be the leading candidate for the generation of novel HPPD inhibitors. Then, synthesis and *At*HPPD inhibition assays were carried out.

3.5. Chemical synthesis and enzyme inhibitory in vitro and Bioassay experiments

The inhibitory activities of compounds **W1**, **W2** and mesotrione on HPPD from different sources are shown in Table 4. The IC$_{50}$ against *At*HPPD in vitro of **W1** was 0.201 μM, analogous to mesotrione (IC$_{50}$ = 0.221 μM). The activity of compound **W1** was greatly increased than the previous screened structure with the pyranone replaced by piperidone (Fu et al., 2018). The IC$_{50}$ of **W2** was 5.221 μM, which was significantly greater than that of mesotrione and compound **W1**. The inhibition of *rice* HPPD and *wheat* HPPD showed that the IC$_{50}$ value of compound **W1** was > 10 μM, almost same as mesotrione, which indicated that compound **W1** might be safe for *rice* HPPD and *wheat* HPPD. Furthermore, compound **W1** did not exhibit the potential to inhibit *h*HPPD activity. Compound **W2** showed good safety in *rice* HPPD, but the estimate was not optimistic for *wheat* HPPD, and it did not have the potential to inhibit *h*HPPD activity.

Therefore, after further structural modification, it was determined that compound **W2** could be developed into HPPD-inhibiting herbicide for *rice* fields, and compound **W1** may serve as a good template for designing effective HPPD inhibitors. After spraying the weeds with mesotrione and the leaves with **W1** for three days, most of the weeds exhibited bleaching symptoms. The leaves, stems and roots of *SF* and *EC* dried up and lost water, accompanied by obvious bleaching symptoms; leaf bleaching also occurs for *AJ* and *AR*, and *DS* and *AR* grow slowly under the same environmental conditions (Fig. 6**A**). Judging from the degree of whitening of *AR*, *AJ* and *DS*, the herbicidal activity of mesotrione was lower than that of **W1**. In vivo safety tests on crops of com-

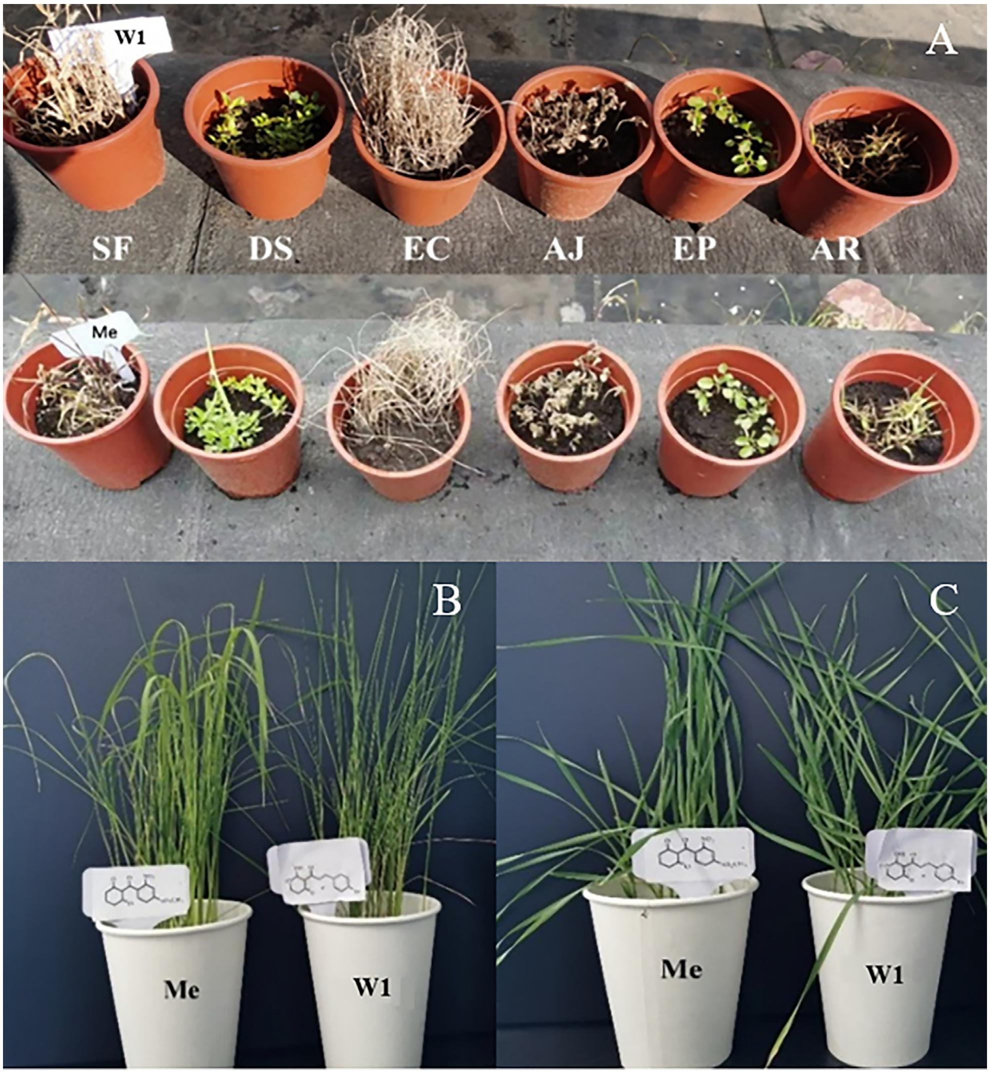

Fig. 6 Bioassay experiment of compound **W1**. (**A**) Bioassay results of compound W1 on weeds: *AJ*, *EP*, *AR*, *SF*, *DS*, and *EC*, (**B**) Bioassay results of compound **W1** on *rice* and (**C**) Bioassay results of compound **W1** on *wheat*.

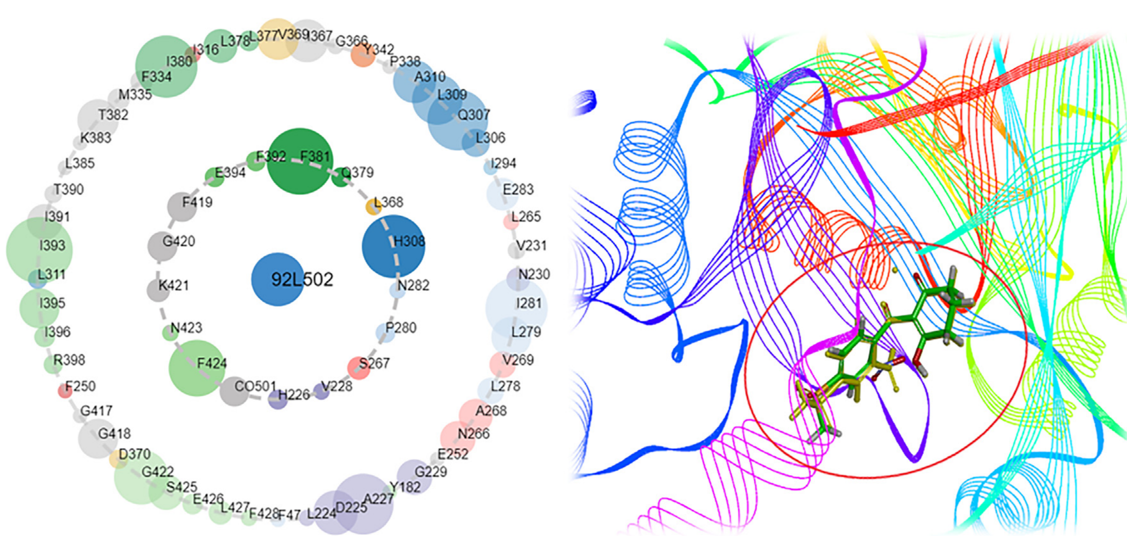

Fig. 7 **(A)** The asteroid plot of ligands and residues and **(B)** Ligand docking diagram in crystal complex.

pound **W1** on *rice* (Fig. 6**B**) and *wheat* (Fig. 6**C**) show that it produces a very invulnerable effect for crops.

3.6. Docking analysis

Molecular docking is the process of studying molecular interactions in drug design. Through the asteroid plot of ligands and residues (Fig. 7**A**) (https://www.mrc-lmb.cam.ac.uk/rajini/index.html), key amino acid interactions were initially obtained. The large circles on the main chain corresponding to Phe424 and Phe381 indicated that the contributions of amino acids Phe424 and Phe381 were substantial. The native and redocked ligands had identical conformations for docking with the binding site, with RMSD being

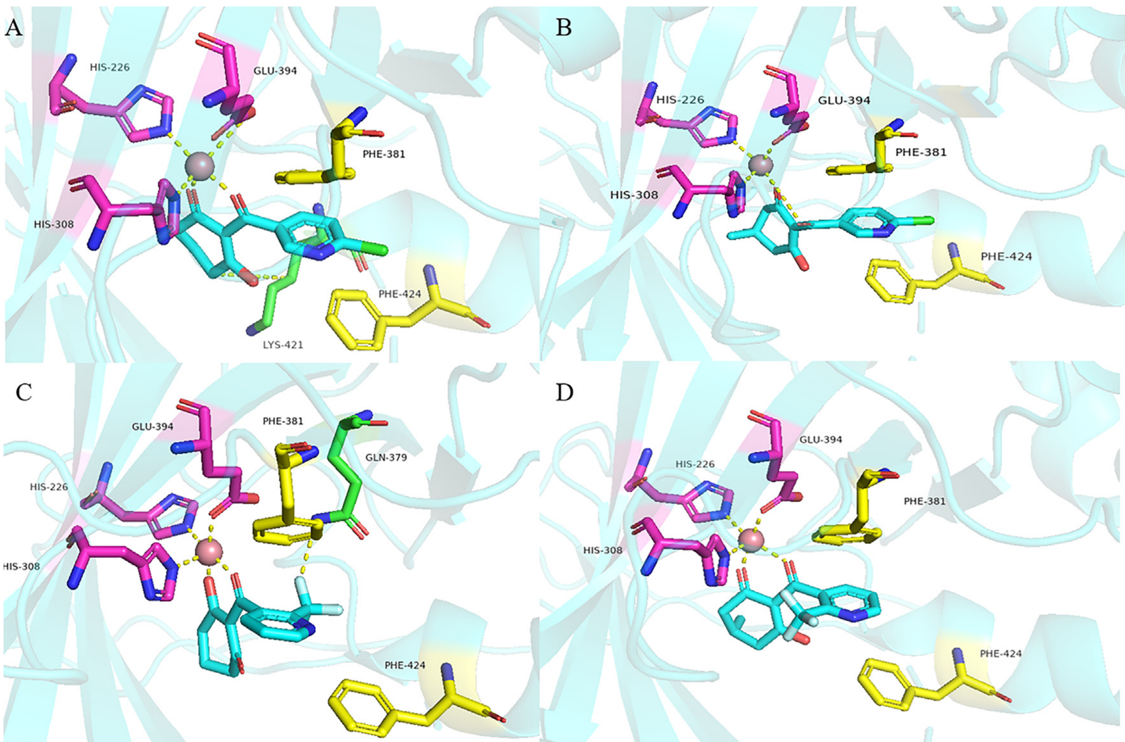

Fig. 8 The QSAR dataset compounds molecular docking in active site **(A)** compound 1, **(B)** compound 3, **(C)** compound 5 and **(D)** compound 6.

Table 5 Docking parameters of the QSAR dataset compounds.

Compound	Structure	-CDOCKER_ ENERGY (kcal mol^{-1})	-Interactive energy (kcal mol^{-1})
1	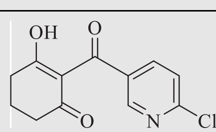	40.27	55.23
3	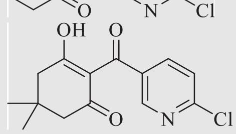	39.72	54.61
5	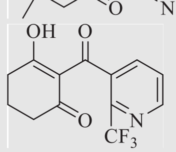	34.95	54.24
6	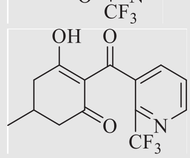	34.21	54.12

of 0.74 (Fig. 7**B**). The re-docked ligand could be well aligned with the ligands in the cocrystallized complex; therefore, the method demonstrated the accuracy and reliability of the docking.

According to the contribution of steric field, compound 3 with bulk substituents (5,5-diCH_3) at the 5-positions (R^1) of the cyclohexanol diketone showed less the pi-alkyl with Lys421 than compound 1 (Fig. 8 **A and B**), which had higher -CDOCKER_ ENERGY and interactive energy than compound 3 (Table 5). The same rule was also observed in compounds 5 and 6. The hydrogen bond of Glu379 between compound 5 and enzyme was not found in compound 6 (Fig. 8**. C and D)**.

All three compounds were well docked into the binding pocket and showed that all the ligands bound to cobalt ions (Fig. 9). The -CDOCKER_ENERGY values of compounds **W1** and **W2** were greater than that of mesotrione, which proved that compounds **W1** and **W2** were expected to be potential HPPD inhibitors. As shown in Fig. 9**A**, mesotrione was entirely embedded in the active pocket and coordinated with Co^{2+} together with His226, His308 and Glu394. Moreover, the benzene ring also formed a sandwich π-π interaction with Phe381 and Phe424, which was conducive to stabilizing the binding protein. The binding mode of compound **W1** is shown in Fig. 9**B**. **W1** bonded with the protein through His226, His308, Glu394, Phe381, Phe392 and Phe424. Compared with the structure of mesotrione, the carbon chain of **W1** was extended by inserting an ethenyl, which made Phe392 and the benzene ring form a new stable π-π interaction, which was more conducive to the structure. Compound **W2** was also well inserted into the active site of the protein (Fig. 9**C**). Compared with mesotrione, compound **W2** introduced an indole ring via bioisosterism of the benzene. The phenyl part of the indole ring formed a sandwich π-π interaction with Phe381 and Phe424, and His308 and the pyrrole subunit of the indole ring also formed a π-π interaction. For the sake of investigating the factors affecting inhibitor activity, MD simulations were carried out.

3.7. MD analysis

MD simulations were performed to analyze the stability of ligand-receptor interactions. The overall stability of the system was monitored by RMSD of backbone atoms (C, Cα, N, and

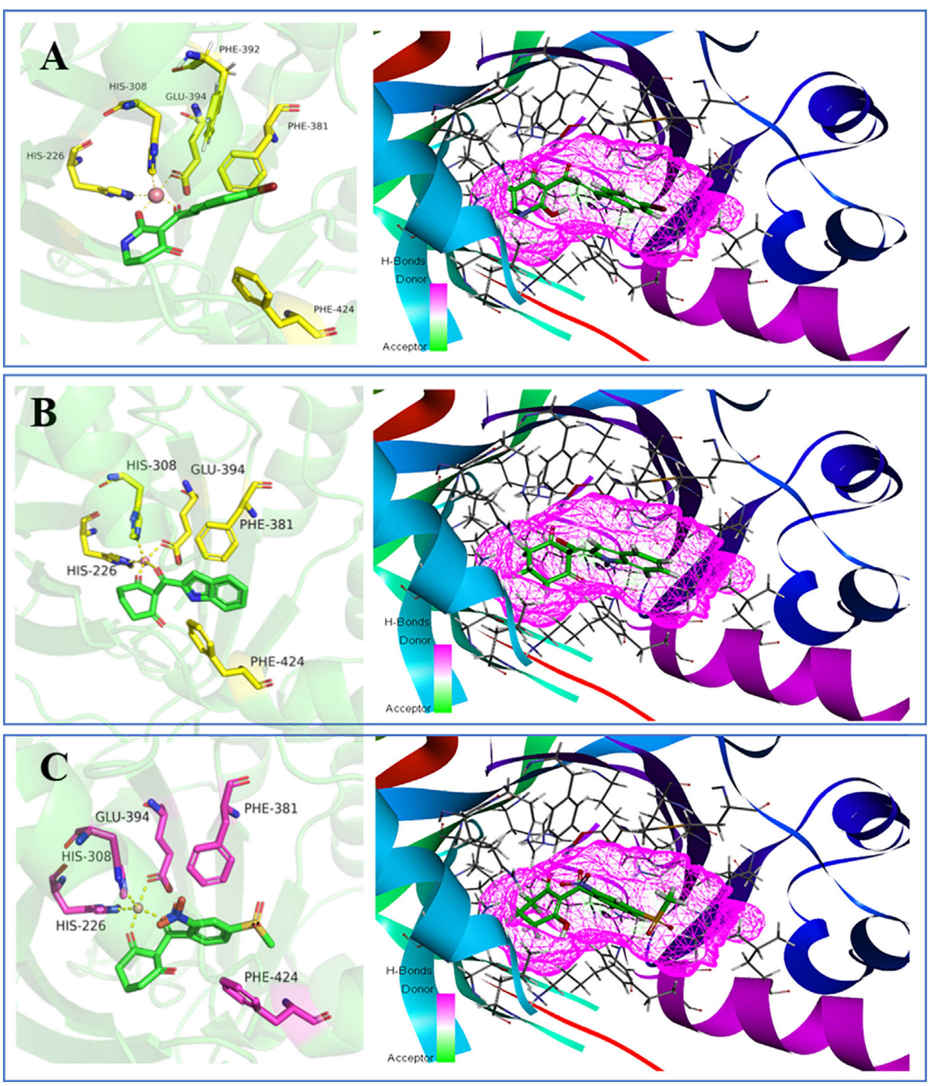

Fig. 9 The receptor–ligand interactions of **(A)** mesotrione, **(B)** compound **W1** and **(C)** compound **W2** at the HPPD binding site.

O) relative to the original docking structure. RMSD value of the backbone Cα atoms was the major parameter used to assess the stability of the system. As Fig. 10**A** shown, the two complexes for HPPD-W1 and HPPD-mesotrione showed slight fluctuations at the start, and then the main chain Cα atoms of the proteins tended to equilibrate after 20 ns. RMSD value of the main chain Cα atoms of compound **W1** was smaller than that of mesotrione, which proved that the skeleton structure of compound **W1** was more stable. Fig. 10**B** illustrates the RMSD value of the protein active pocket with residues 5 Å around the ligand. In the entire MD simulation process, all compounds were relatively stable. Fig. 10**C** showed that all the heavy atoms in the ligand balanced within the final 5 ns, indicating that all systems reached the steady state in the course of simulation.

The calculated MM-PBSA was given in Table 6. ΔG_{bind} reflected the degree of binding between the compound and the protein. The ΔG_{bind} values of the hit compounds **W1**, **W2** and mesotrione were −44.590, −28.001 and −35.560 kcal mol^{-1}, respectively. The calculated results indicated that the binding ability of **W1** with protein was better than that of mesotrione. The ΔE_{vdw}, ΔE_{ele} and ΔG_{SA} values calculated by MM-PBSA were the positive contributions to ΔG_{bind}, while ΔG_{PB} weakened the binding process. It was found that the ΔE_{vdw} value of compound **W1** (-37.491 kcal mol^{-1}) was comparatively lower than that of mesotrione (-36.423 kcal mol^{-1}).

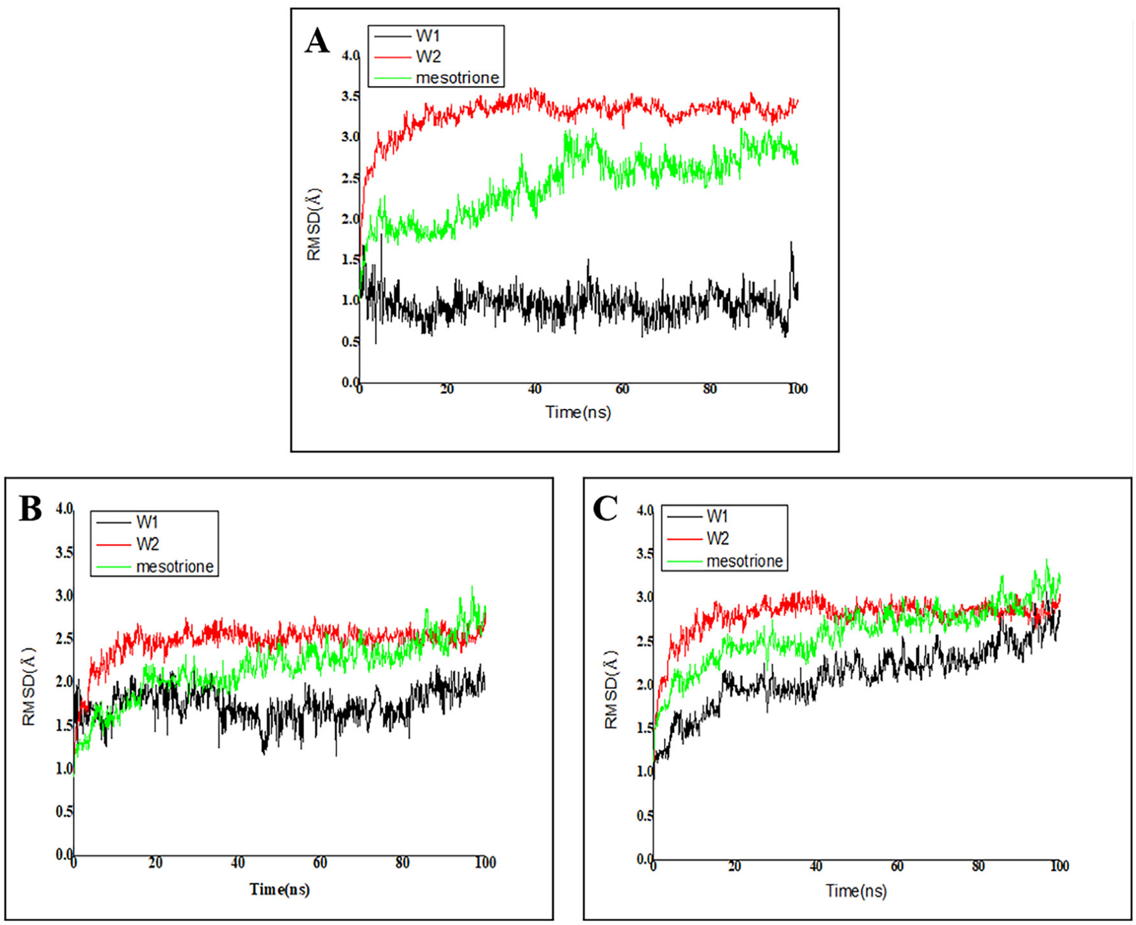

Fig. 10 Protein-ligand RMSD of **(A)** Cα atoms. **(B)** Side chains and **(C)** heavy atoms.

Table 6 Binding free energies (kcal mol^{-1}) of compounds **W1** and **W2**.

Compound	ΔE_{vdw}	ΔE_{ele}	ΔG_{PB}	ΔG_{SA}	ΔE_{MM}	ΔG_{sol}	ΔG_{bind}
W1	−37.491	−31.226	25.521	−1.394	−68.717	24.127	−44.590
W2	−41.861	−26.801	41.770	−1.109	−68.662	40.661	−28.001
Mesotrione	−36.423	−32.947	33.179	−0.631	−69.370	33.810	−35.560

ΔE_{vdw}, van der Waals energy; ΔE_{ele}, electrostatic energy; ΔG_{PB}, polar solvation energy with the PB model; ΔG_{SA}, nonpolar solvation energy with the PB model; ΔE_{MM}, interaction energy; ΔG_{sol}, solvation contribution;
$\Delta E_{\mathrm{MM}} = \Delta E_{\mathrm{vdw}} + \Delta E_{\mathrm{ele}}$; $\Delta G_{\mathrm{sol}} = \Delta G_{\mathrm{PB}} + \Delta G_{\mathrm{SA}}$; $\Delta G_{bind} = \Delta E_{\mathrm{vdw}} + \Delta E_{\mathrm{ele}} + \Delta G_{\mathrm{PB}} + \Delta G_{\mathrm{SA}}$.

Table 7 The ADMET predictions of compounds **W1** and **W2.**

No.	W1	W2	Mesotrione
Solubility Level	3	3	3
PPB# Prediction	True	True	True
Hepatotoxic	−2.89	−1.25	−6.39
Aerobic Biodegradability	Degradable	Degradable	Degradable
Mutagenicity	Non-Mutagen	Non-Mutagen	Non-Mutagen
Carcinogenicity	Non-Carcinogen	Non-Carcinogen	Non-Carcinogen
Skin irritancy	None	None	None
CYP2D6_Applicability	12.74	10.12	18.14
DTP Prediction	Non-Toxic	Non-Toxic	Non-Toxic

Solubility Level: Categorical solubility level. 2: Yes, low; 3: Yes, good.
Hepatotoxic: <-0.4095: nontoxic; >-0.4095: toxic.
PPB: Plasma Protein Binding ability. < -2.209: $\geq 90\%$, false; >-2.209: $\leq 90\%$, true.

The nonpolar solvation of compound **W1** ($\Delta E_{vdw} + \Delta G_{SA}$ = -38.885 kcal mol^{-1}) was slightly better than that of mesotrione (-37.054 kcal mol^{-1}). Therefore, the above results confirmed that nonpolar interactions made a lot of sense to strengthen binding affinities of molecules with the protein system.

3.8. ADMET

The obtained compounds **W1** and **W2** were analyzed using ADMET (Table 7). The ADMET properties for the two compounds were all within the safety ranges for human beings., The compound would be a lower possibility of liver toxicity if the Bayesian score in the hepatotoxicity model was less than −0.4095. Therefore, the three compounds were determined to possess very low hepatotoxicity. The PPB model was a significant indicator of drug distribution. However, the three compounds met the critical fraction of −2.209 for highly combined use with plasma proteins. The CYP2D6_Applicability parameter indicated mesotrione = 18.140, **W1** = 12.745, and **W2** = 10.122. All properties and three components were within expected ranges. The premise of a medicine is to satisfy the absorptive, distributional, metabolic, excretory and, most importantly, nontoxic requirements in vivo. For pesticides, nontoxicity is the key consideration, but the nature of ADME in the body is still not negligible.

Compounds **W1**, **W2** and mesotrione were determined to be relatively safe through assessments of toxicity prediction, carcinogenicity, mutagenicity and skin irritation and were found to be aerobically and biodegradable. All in all, compounds **W1** and **W2** are expected to become new HPPD inhibitors due to their excellent solubility, degradability, and lack of mutagenicity, carcinogenicity, and skin irritation.

4. Conclusion

CoMFA and CoMSIA models with perfect cross-validated correlation coefficient values were built based on 36 pyridine derivatives. The effects associated with each substituent were predicted in the molecular skeleton, leading to better insights for designing new HPPD inhibitors. Two newly designed compounds, **W1** and **W2,** were synthesized and subjected to *At*HPPD inhibition and bioassay verification. Molecular docking experiments verified the binding mode of the novel compounds at the HPPD active pocket. Compound **W1** showed satisfactory inhibitory activity with IC_{50} being 0.201 μM. *AJ*, *AR*, *SF* and *EC* showed bleaching symptoms after treatment with leaf spray. MD simulation and MM-PBSA energy calculation confirmed that the binding efficiency of compound **W1** to the enzyme was high. ADMET prediction showed that these two newly designed compounds had excellent physicochemical properties, low toxicity and weak side effects. The above work supplied theoretical guidance and practical application for designing novel HPPD inhibitors with powerful activity.

CRediT authorship contribution statement

Juan Shi: Methodology, Software, Formal analysis, Investigation, Writing – original draft. **Li-Xia Zhao:** Project administration. **Jia-Yu Wang:** Formal analysis, Visualization, Investigation. **Tong Ye:** Resources, Data curation. **Meng Wang:** Validation. **Shuang Gao:** Visualization, Investigation. **Fei Ye:** Supervision, Conceptualization, Writing – review & editing. **Ying Fu:** Supervision, Funding acquisition, Writing – review & editing.

Acknowledgement

This work was supported by the National Nature Science Foundation of China (22077014). The authors are grateful to Prof. Jian Wang (Shenyang Pharmaceutical University) for helping in the application of SYBYL software.

Appendix A. Supplementary material

Supplementary data to this article can be found online at https://doi.org/10.1016/j.arabjc.2022.103919.

References

Aouidate, A., Ghaleb, A., Ghamali, M., Chtita, S., Oussa, A., Choukrad, M., Sbai, A., Bouachrine, M., Lakhlifi, T., 2018. Furanone derivatives as new inhibitors of CDC7 kinase: development of structure activity relationship model using 3D QSAR, molecular docking, and in silico ADMET. Struct Chem. 29, 1031–1043. https://doi.org/10.1007/s11224-018-1086-4.

Beaudegnies, R., Emunds, A.J.F., Fraser, T.M., Hall, R.G., Hawkes, T.R., Mitchell, G., Schaetzer, J., Wendeborn, S., Wibley, J., 2009. 4-Hydroxyphenylpyruvate dioxygenase inhibitors-a review of the triketone chemistry story from a syngenta perspective. Bioorgan. Med. Chem. 17, 4134–4152. https://doi.org/10.1016/j.bmc.2009.03.015.

Dong, H.H., Liu, J., Liu, X.R., Yu, Y.Y., Cao, S.W., 2017. Combining molecular docking and QSAR studies for modeling the anti-tyrosinase activity of aromatic heterocycle thiosemicarbazone analogues. J. Mol. Struct. 1151, 353–365. https://doi.org/10.1016/j.molstruc.2017.08.034.

Fu, Y., Liu, Y.X., Kang, T., Sun, Y.N., Li, J.Z., Ye, F., 2019a. Identification of novel inhibitors of p-hydroxyphenylpyruvate dioxygenase using receptor-based virtual screening. J. Taiwan. Inst. Chem. Eng. 103, 33–43. https://doi.org/10.1016/j.jtice.2019.08.005.

Fu, Y., Liu, Y.X., Yi, K.H., Li, M.Q., Li, J.Z., Ye, F., 2019b. Quantitative structure activity relationship studies and molecular dynamics simulations of 2-(aryloxyacetyl) cyclohexane-1,3-diones derivatives as 4-hydroxyphenylpyruvate dioxygenase inhibitors. Front. Chem. 7, 556. https://doi.org/10.3389/fchem.2019.00556.

Fu, Y., Sun, Y.N., Yi, K.H., Li, M.Q., Cao, H.F., Li, J.Z., F, Ye., 2018. Combination of virtual screening protocol by in silico toward the discovery of novel 4-hydroxyphenylpyruvate dioxygenase inhibitors. Front. Chem. 6, 14. https://doi.org/10.3389/fchem.2018.00014.

Fu, Y., Wang, M., Zhao, L.X., Zhang, S.Q., Liu, Y.X., Guo, Y.Y., Zhang, D., Gao, S., Ye, F., 2021. Design, synthesis, herbicidal activity and CoMFA of novel aryl-formyl piperidinone HPPD inhibitors. Pestic Biochem Physiol. 174,. https://doi.org/10.1016/j.pestbp.2021.104811 104811.

Fu, Y., Ye, T., Liu, Y.X., Wang, J., Ye, F., 2020. Based on the virtual screening of multiple pharmacophores, docking and molecular dynamics simulation approaches toward the discovery of novel hppd inhibitors. Int. J. Mol. Sci. 21 (15), 5546. https://doi.org/10.3390/ijms21155546.

Fu, Y., Zhang, S.Q., Liu, Y.X., Wang, J.Y., Gao, S., Zhao, L.X., Ye, F., 2019c. Design, synthesis, SAR and molecular docking of novel green niacin-triketone HPPD inhibitor. Ind. Crops Prod. 137, 566–575. https://doi.org/10.1016/j.indcrop.2019.05.070.

Ganesan, K., Ponya, U.P., Dharmasivam, M., Natarajan, R., 2018. Exploring the DNA interactions, FGF growth receptor interaction and biological screening of metal (II) complexes of NNN donor ligand derived from 2-(aminomethyl)benzimidazole. J. Biol. Macromol. 126, 1303–1317. https://doi.org/10.1016/j.ijbiomac.2018.09.116.

He, B., Dong, J., Lin, H.Y., Wang, M.Y., Li, X.K., Zheng, B.F., Chen, Q., Hao, G.F., Yang, W.C., Yang, G.F., 2019. Pyrazole-isoindoline-1,3-dione hybrid: a promising scaffold for 4-hydroxyphenylpyruvate dioxygenase inhibitors. J. Agric. Food Chem. 67, 10844–10852. https://doi.org/10.1021/acs.jafc.9b04917.

He, B., Wu, F.X., Yu, L.K., Wu, L., Chen, Q., Hao, G.F., Yang, W. C., Lin, H.Y., Yang, G.F., 2020. Discovery of novel pyrazole-quinazoline-2,4-dione hybrids as 4-hydroxyphenylpyruvate dioxygenase inhibitors. J. Agric. Food Chem. 68, 5059–5067. https://doi.org/10.1021/acs.jafc.0c00051.

Huang, L.L., Han, J., Ran, X.J., Chen, X.P., Wang, Z.H., Wu, F.H., 2018. 3D-QSAR, molecular docking and molecular dynamics simulations of oxazepane amidoacetonitrile derivatives as novel DPPI inhibitors. J. Mol. Struct. 1168, 223–233. https://doi.org/10.1016/j.molstruc.2018.05.025.

Hu, W., Gao, S., Zhao, L.X., Guo, K.L., Wang, J.Y., Gao, Y.C., Shao, X.X., Fu, Y., Ye, F., 2022. Design, synthesis and biological activity of novel triketone-containing quinoxaline as hppd inhibitor. Pest Manag. Sci. 78, 938–946. https://doi.org/10.1002/ps.6703.

Jia, C.Y., Li, J.Y., Hao, G.F., Yang, G.F., 2019. A drug-likeness toolbox facilitates ADMET study in drug discovery. Drug Discov. Today. 25, 248–258. https://doi.org/10.1016/j.drudis.2019.10.014.

Jiang, D.H., Chen, J.X., Zan, N.N., Li, C.Y., Hu, D.Y., Song, B.A., 2021. Discovery of novel chromone derivatives containing a sulfonamide moiety as anti-ToCV agents through the tomato chlorosis virus coat protein-oriented screening method. J. Agric. Food Chem. 41, 12126–12134. https://doi.org/10.1021/acs.jafc.1c02467.

Kothandan, G., Gadhe, C.G., Madhavan, T., Cho, S.J., 2011. Binding site analysis of CCR2 through in silico methodologies: docking, CoMFA, and CoMSIA. Chem. Biol. Drug Des. 78, 161–174. https://doi.org/10.1111/j.1747-0285.2011.01095.x.

Li, L., Gao, S., Yang, L., Liu, Y.L., Li, P., Ye, F., Fu, Y., 2021. Cobalt (II) complex as a fluorescent sensing platform for the selective and sensitive detection of triketone HPPD inhibitors. J. Hazard. Mater. 404,. https://doi.org/10.1016/j.jhazmat.2020.124015 124015.

Liang, W.K., Zhang, W.W., Lv, Z.M., Li, C.H., 2020. 4-Hydroxyphenylpyruvate dioxygenase from sea cucumber Apostichopus japonicus negatively regulates reactive oxygen species production. Fish Shellfish Immunol. 101, 261–268. https://doi.org/10.1016/j.fsi.2020.04.013.

Lin, H.Y., Chen, X., Chen, J.N., Wang, D.W., Wu, F.X., Lin, S.Y., Zhan, C.G., Wu, J.W., Yang, W.C., Yang, G.F., 2019a. Crystal structure of 4-hydroxyphenylpyruvate dioxygenase in complex with substrate reveals a new starting point for herbicide discovery. Research. 2019, 2602414. https://doi.org/10.34133/2019/2602414.

Lin, H.Y., Chen, X., Dong, D., Yang, J.F., Xiao, H., Ye, Y., Li, L.H., Zhan, C.G., Yang, W.C., Yang, G.F., 2021. Rational redesign of enzyme via the combination of quantum mechanics/molecular mechanics, molecular dynamics, and structural biology study. J. Am. Chem. Soc. 143, 15674–15687. https://doi.org/10.1021/jacs.1c06227.

Lin, H.Y., Yang, J.F., Wang, D.W., Hao, G.F., Dong, J.Q., Wang, Y. X., Yang, W.C., Wu, J.W., Zhan, C.G., Yang, G.F., 2019b. Molecular insights into the mechanism of 4-hydroxyphenylpyruvate dioxygenase inhibition: enzyme kinetics, X-ray crystallography and computational simulations. FEBS. J. 286, 975–990. https://doi.org/10.1111/febs.14747.

Liu, Y.Y., Ding, T.T., Feng, X.Y., Xu, W.R., Cheng, X.C., 2019. Virtual identification of novel peroxisome proliferator-activated receptor (PPAR) alpha/delta dual antagonist by 3D-QSAR, molecule docking and molecule dynamics simulation. J. Biomol. Struct. Dyn. 38, 4143–4161. https://doi.org/10.1080/07391102.2019.1673211.

Mohd, S., Ruben, C., Melanie, G., Samantha, S., Alan, C., 2019. Structure based identification of novel inhibitors against ATP synthase of mycobacterium tuberculosis: a combined in silico and in vitro study. Int. J. Biol. Macromol. 135, 582–590. https://doi.org/10.1016/j.ijbiomac.2019.05.108.

Moran, G.R., 2014. 4-Hydroxyphenylpyruvate dioxygenase and hydroxymandelate synthase: exemplars of the α-keto acid dependent oxygenases. Arch. Biochem. Biophys. 544, 58–68. https://doi.org/10.1016/j.abb.2013.10.022.

Nan, J.X., Yang, J.F., Lin, H.Y., Yan, Y.C., Zhou, S.M., Wei, X.F., Chen, Q., Yang, W.C., Qu, R.Y., Yang, G.F., 2021. Synthesis and herbicidal activity of triketone-aminopyridines as potent p-hydroxyphenylpyruvate dioxygenase inhibitors. J. Agric. Food Chem. 69, 5735–5745. https://doi.org/10.1021/acs.jafc.0c07782.

Ndikuryayo, F., Moosavi, B., Yang, W.C., Yang, G.F., 2017. 4-Hydroxyphenylpyruvate dioxygenase inhibitors: from chemical biology to agrochemicals. J. Agric. Food Chem. 65, 8523–8537. https://doi.org/10.1021/acs.jafc.7b03851.

Neidig, M.L., Kavana, M., Moran, G.R., Solomon, E.I., 2004. CD and MCD studies of the non-heme ferrous active site in (4-hydroxyphenyl) pyruvate dioxygenase: correlation between oxygen activation in the extradiol and alpha-KG-dependent dioxygenases. J. Am. Chem. Soc. 126, 4486–4487. https://doi.org/10.1021/ja0316521.

Qu, R.X., Nan, J.X., Yan, Y.C., Chen, Q., Ndikuryayo, F., Wei, X.F., Yang, W.C., Lin, H.Y., Yang, G.F., 2021. Structure-guided discovery of silicon-containing subnanomolar inhibitor of hydroxyphenylpyruvate dioxygenase as a potential herbicide. J. Agric. Food Chem. 69, 459–473. https://doi.org/10.1021/acs.jafc.0c03844.

Raspail, C., Graindorge, M., Moreau, Y., Crouzy, S., Lefebvre, B., Robin, A.Y., Dumas, R., Matringe, M., 2011. 4-Hydroxyphenylpyruvate dioxygenase catalysis: identification of catalytic residues and production of a hydroxylated intermediate shared with a structurally unrelated enzyme. J. Biol. Chem. 286, 26061–26070. https://doi.org/10.1074/jbc.M111.227595.

Sabine, K., Florian, S.J., Bernd, F.L., Gudrun, L., Daniel, P., Sabrina, K., Marc, L., Arno, S., von Pascal, K.-D., Sebastian, K., Sascha, G., 2020. Aclonifen targets solanesyl diphosphate synthase, representing a novel mode of action for herbicides. Pest Manag. Sci. 76 (10), 3377–3388. https://doi.org/10.1002/ps.5781.

Shaner, D.L., 2004. Herbicide safety relative to common targets in plants and mammals. Pest Manag. Sci. 60, 17–24. https://doi.org/10.1002/ps.782.

Singh, A., Goyal, S., Jamal, S., Subramani, B., Das, M., Admane, N., Grover, A., 2016. Computational identification of novel piperidine derivatives as potential HDM2 inhibitors designed by fragment-based QSAR, molecular docking and molecular dynamics simulations. Struct. Chem. 27, 993–1003. https://doi.org/10.1007/s11224-015-0697-2.

Singh, D., Kumar, J., Kumar, A., 2018. Isolation of pyomelanin from bacteria and evidences showing its synthesis by 4-hydroxyphenylpyruvate dioxygenase enzyme encoded by hppd gene. Int. J. Biol. Macromol. 119, 864–873. https://doi.org/10.1016/j.ijbiomac.2018.08.003.

Song, H.M., Zhao, L.X., Zhang, S.Q., Ye, T., Fu, Y., Ye, F., 2021. Design, synthesis, structure-activity relationship, molecular docking, and herbicidal evaluation of 2-cinnamoyl-3-hydroxycyclohex-2-en-1-one derivatives as novel 4-hydroxyphenylpyruvate dioxygenase inhibitors. J. Agric. Food Chem. 69, 12621–12633. https://doi.org/10.1021/acs.jafc.1c04621.

Sushil, P., Thamer, A.B., Abdus, S., Mohammad, N.S., Rahat, A., Md, A.-A.-M., Zulkar, N., Rahman, I.R., Kabir, T.M.E., Islam, T. M.M., Saddam, H.M., Tomasz, M.K., Foysal, A., Ishtiaq, Q., Shahedur, R.M., 2021. Spike protein recognizer receptor ACE2 targeted identification of potential natural antiviral drug candidates against SARS-CoV-2. Int. J. Biol. Macromol. 191, 1114–1125. https://doi.org/10.1016/j.ijbiomac.2021.09.146.

Tang, H.J., Yang, L., Li, J.H., Chen, J., 2016. Molecular modelling studies of 3,5-dipyridyl-1,2,4-triazole derivatives as xanthine oxidoreductase inhibitors using 3D-QSAR, Topomer CoMFA, molecular docking and molecular dynamic simulations. J. Taiwan. Inst. Chem. Eng. 68, 64–73. https://doi.org/10.1016/j.jtice.2016.09.018.

Wang, D.W., Lin, H.Y., Gao, R.J., Yang, S.G., Chen, Q., Hao, G.F., Yang, W.C., Yang, G.F., 2014. Synthesis and herbicidal evaluation of triketone-containing quinazoline-2,4-diones. J. Agric. Food Chem. 62, 11786–11796. https://doi.org/10.1021/jf5048089.

Wang, F., Yang, J.F., Wang, M.Y., Jia, C.Y., Shi, X.X., Hao, G.F., Yang, G.F., 2020a. Graph attention convolutional neural network model for chemical poisoning of honey bees' prediction. Sci. Bull. 65, 1184–1191. https://doi.org/10.1016/j.scib.2020.04.006.

Wang, J.L., Cheng, L.P., Wang, T.C., Deng, W., Wu, F.H., 2017. Molecular modeling study of CP-690550 derivatives as JAK3 kinase inhibitors through combined 3D-QSAR, molecular docking, and dynamics simulation techniques. J. Mol. Graph. Model. 72, 178–186. https://doi.org/10.1016/j.jmgm.2016.12.020.

Wang, M.M., Huang, H., Shu, L., Liu, J.M., Zhang, J.Q., Yan, Y.L., Zhang, D.Y., 2020b. Synthesis and herbicidal activities of aryloxyacetic acid derivatives as HPPD inhibitors. Beilstein. J. Org. Chem. 16, 233–247. https://doi.org/10.3762/bxiv.2019.150.v1.

Wang, X.N., Lin, H.Y., Liu, J.J., Zhao, X.Y., Chen, X., Yang, W.C., Yang, G.F., 2021. The structure of 4-hydroxylphenylpyruvate dioxygenase complexed with 4-hydroxylphenylpyruvic acid reveals an unexpected inhibition mechanism. Chin. Chem. Lett. 32, 1920–1924. https://doi.org/10.1016/j.cclet.2021.02.041.

Wang, Y.L., Wang, F., Shi, X.X., Jia, C.Y., Wu, F.X., Hao, G.F., Yang, G.F., 2020c. Cloud 3D-QSAR: a web tool for the development of quantitative structure–activity relationship models in drug discovery. Brief Bioinform. 22, 276. https://doi.org/10.1093/bib/bbaa276.

Xing, S.S., Chen, Y., Xiong, B.C., Lu, W.X., Li, Q., Wang, Y.Y., Jiao, M.X., Feng, F., Chen, Y., Liu, W.Y., Sun, H.P., 2020. Synthesis and bio-evaluation of a novel selective butyrylcholinesterase inhibitor discovered through structure-based virtual screening. Int. J. Biol. Macromol. 166, 1352–1364. https://doi.org/10.1016/j.ijbiomac.2020.11.015.

Yang, J.F., Wang, F., Chen, Y.Z., Hao, G.F., Yang, G.F., 2019. LARMD: integration of bioinformatic resources to profile ligand-driven protein dynamics with a case on the activation of estrogen receptor. Brief Bioinform. 21, 2206–2218. https://doi.org/10.1093/bib/bbz141.

Zhang, L., Tan, Y., Wang, N.X., Wu, Q.Y., Xi, Z., Yang, G.F., 2010. Design, syntheses and 3D-QSAR studies of novel N-phenyl pyrrolidin-2-ones and N-phenyl-1H-pyrrol-2-ones as protoporphyrinogen oxidase inhibitors. Bioorg. Med. Chem. 18, 7948–7956. https://doi.org/10.1016/j.bmc.2010.09.036.